Influence of Measurement Cell on Predicted Attrition by the Distinct Element Method

C.L. Hare, M. Ghadiri
Institute of Particle Science and Engineering, University of Leeds, Leeds, LS2 9JT

Abstract

During agitated drying and mixing processes, particle beds are exposed to shear deformation. This leads to particle attrition, the extent of which is dependent on the prevailing stresses and strains in the bed. The distributions of shear stresses and strain rates within the bed are highly non-uniform, requiring attention to localised conditions. Therefore a narrow angular sector of the bed is divided radially and vertically into a number of measurement cells, within which the stresses and strain rates are calculated throughout one rotation by the Distinct Element Method. These are then used in an empirical relationship of material breakage to predict the extent of attrition due to agitation. Here we investigate the influence of the measurement cell size on the estimated stresses and strain rates, and the subsequent effect on the predicted attrition. The measurement cell size is altered by varying the measurement sector size and the number of radial and vertical divisions within it. The median particle size is also varied to establish its influence on the predicted attrition. An increase in the average number of particles in a given cell, by varying the particle size or measurement cell dimensions, leads to a reduction in the estimated stresses and strain rates, and therefore a reduction in the predicted attrition. Comparison of the predicted attrition with the experimental breakage in the agitated vessel shows that the prediction method is accurate when the cell dimensions are comparable to the width of a naturally occurring shear band.

Keywords: attrition, prediction, DEM, simulation, shear

1. Introduction

During processing and handling, particles are exposed to forces that may cause unwanted breakage, commonly referred to as attrition. This can occur through sliding, impact and, most commonly, shear deformation. In many particle processes, such as mixing/blending, granulation and discharge from hoppers, transitions from stationary state to flow are present. Particles are exposed to shear deformation within the transition region, which typically has a width in the range of 5 – 10 particle diameters [1]. The bed must dilate within this region to allow flow; consequently significant shear stresses are developed and breakage may occur by abrasion, wear, erosion and fragmentation. The occurrence and extent of breakage are dependent on the prevailing stresses to which the particles are exposed and the resistance of the particles to these stresses.

Particles experience stress due to force transmission through contacts with processing equipment and other particles. The precise locations, directions and magnitudes of these contact forces within a bed are transient and highly dependent on the positions and

orientations of individual particles, otherwise known as the bed fabric [2]. Due to particle size and shape distributions, and a lack of knowledge of the precise position and orientation of the particles within a bed, the estimation of the contact forces in a particle bed is challenging. Furthermore, particles always have a strength distribution, hence a rigorous mechanistic model to describe particle breakage under shear deformation has yet to be developed. Developments in the Distinct Element Method (DEM) have enabled the force networks within a sheared bed to be estimated reliably for spherical particles [3-5]. Its potential to predict experimental breakage caused by shearing has also been demonstrated [6].

A number of empirical relationships have been developed to describe attrition due to shear deformation [7-10]. The model of Neil and Bridgwater [11], as given by Eq. 1, has been shown to provide the best fit to the widest range of stresses, strains and material types [10-12].

$$W = k_N \left[\left(\frac{\sigma}{\sigma_{SCS}} \right) \Gamma^{\varphi} \right]^{\beta} \tag{1}$$

where W is the extent of attrition, σ and Γ are the applied stress and strain, respectively, σ_{SCS} is the material side-crushing strength, and k_N, φ and β are material dependent parameters. Hare *et al.* [13] proposed a method to predict attrition in agitated particle beds by estimating the prevailing stresses and strains throughout the bed and applying a model of attrition to these beds conditions. A modified form of the Neil and Bridgwater relationship (Eq. 1) was used to relate the attrition to the prevailing stresses and strains (see section 2) throughout the bed, which were in turn estimated using DEM. Within the DEM simulations, the radial and vertical variations of stress and strain rate were estimated from the contact forces and particle velocities in an array of measurement cells. However, these estimations are dependent on the dimensions of the chosen measurement cells. Therefore, in this current work we analyse the influence of the measurement cell dimensions on the predicted stresses, strain rates and overall attrition within the agitated particle bed.

2. Materials and methods

A summary of the attrition prediction method proposed by Hare *et al.* [13] is given here. The agitated particle bed is simulated using DEM. The macroscopic forces in the simulation are validated by the impeller torque measurement, and the particle velocity distribution is validated by Positron Emission Particle Tracking (PEPT), as shown in [13]. These validations, along with the rationale for the properties of the simulated materials are detailed in [13]. The properties of the simulated and experimental materials are shown in Table 1.

The simulated bed is divided into a number of measurement cells (Figure 1), within which all normal forces acting on each particle are considered to estimate the normal stresses,

$$\sigma_{ii} = \frac{1}{V}\sum_{1}^{N} F_{ii}.r_p \tag{2}$$

where V is the total volume of the cell, N is the number of particles in the cell, F is the force acting in direction i on face i of the particle (the directions are defined in Figure 2), and r_p is the particle radius [14]. From these normal stresses the deviatoric stress, τ_D, within each cell is established by Eq. 3 [15]:

$$\tau_D = \frac{\sqrt{\left(\sigma_{xx}-\sigma_{yy}\right)^2+\left(\sigma_{xx}-\sigma_{zz}\right)^2+\left(\sigma_{yy}-\sigma_{zz}\right)^2}}{\sqrt{6}} \tag{3}$$

To calculate strain rate in each cell, cylindrical coordinate system is used due to the axi-symmetrical bed geometry. The strain rate, γ, within a cell is given by Eq. 4 [16], from which the strain is calculated.

$$\gamma = \frac{1}{2}\sqrt{\left(\frac{\partial v_\theta}{\partial r}-\frac{v_\theta}{r}\right)^2+\left(\frac{\partial v_\theta}{\partial z}\right)^2} \tag{4}$$

where v_θ is the average particle velocity in the θ direction. The estimation of stress and strain is carried out at a number of intervals over the period of one impeller rotation, once the bed is deemed to have reached steady-state. The particle breakage after shearing at a range of stresses and strains is established experimentally in an annular shear cell, and the modified form of the relationship of Neil and Bridgwater [11] based on the shear stress (given by Eq. 5) is then fitted to the results.

$$W = K_N\left[\left(\frac{\tau}{\tau_{ref}}\right)\Gamma^{\varphi}\right]^{\beta} \tag{5}$$

where τ_{ref} is the characteristic shear strength of the material, and K_N, φ and β are empirically determined constants. This empirical relationship is then coupled with the estimation of stress and strain rate distributions to predict the attrition throughout one impeller rotation,

$$W_{I=1} = K_N\sum_{1}^{c}\sum_{1}^{n}\left(\chi_{c,n}\left[\frac{\tau_{c,n}}{\tau_{ref}}\right]^{\beta}\left[\left(\sum_{1}^{n}\left(\Gamma_{c,n}\right)^{\varphi\beta}\right)-\left(\sum_{1}^{n-1}\left(\Gamma_{c,n}\right)^{\varphi\beta}\right)\right]\right) \tag{6}$$

and

$$\Gamma_{c,n} = \int_{t_A}^{t_B}\left(\gamma_{c,n}dt\right) \tag{7}$$

where $\chi_{c,n}$ is the mass fraction in cell, c, at measurement interval, n, and t_A and t_B are the times at the start and end of the measurement interval [13]. Given that the bed is in a cyclic steady-

state regime from a stress view point, the distribution of stresses and strain rates remain unchanged throughout subsequent impeller rotations. Consequently the attrition is predicted for *I* rotations by:

$$W_I = K_N \sum_{1}^{c} \sum_{1}^{n} \left(\chi_{c,n} \left[\frac{\tau_{c,n}}{\tau_{ref}} \right]^{\beta} \left[\left(\sum_{1}^{n} \left(I \cdot \Gamma_{c,n} \right)^{\varphi\beta} \right) - \left(\sum_{1}^{n-1} \left(I \cdot \Gamma_{c,n} \right)^{\varphi\beta} \right) \right] \right) = W_{I=1} \cdot I^{\varphi\beta} \quad (8)$$

The attrition of a 250 g bed of Paracetamol particles, with an approximate bed height of 50 – 60 mm, in a cylindrical vessel of 94 mm diameter, agitated by a vertical-axis, retreat-curve impeller was considered in the work of Hare *et al.* [13]. Particles were sieved to the 500 – 600 µm size range prior to agitation in the vessel or shearing in the shear cell. The attrition was calculated as the mass percentage of material that passed through a sieve that was two standard sizes below the feed size, in this case a 355 µm sieve. In the present work, the influence of the measurement cell size on the estimated stress and strain rate distribution is considered. The number of radial and vertical divisions are set to be equal. It is designated by n_d and varied between the values of 2, 3 and 4. The measurement sector size, θ_{sec}, is set at 10^o, 25^o and 40^o. For the initial conditions of $n_d = 3$ and $\theta_{sec} = 25^o$, the median simulated particle size is 2, 3 or 4 mm, whilst the span of the size distribution remains constant and equal to that of the experimental material (0.18). Due to computational power and memory limitations, the particle size used in DEM simulations is much larger than the actual particle size in experiments. However, scaling up of particle size in DEM simulations has been shown to be able to provide suitable velocity measurements when suitable scaling criteria are maintained [13, 17 – 18]. The simulation condition sets are shown in Table 2.

Table 1. Experimental and simulated material properties

Experiment		**Simulation**	
Property	**Value**	**Property**	**Value**
Paracetamol:			
		Number of particles	13500
Density, ρ (kg/m^3)	1300	Density, ρ (kg/m^3)	1300
Sieve size, d_s (μm)	500 – 600	Diameter, d_{med} (mm)	2, 3, 4
Shear modulus, E (GPa)	11	Normal stiffness, K_n (N/m)	1.2×10^5
Poisson's Ratio, v	0.3	Shear stiffness, K_s (N/m)	9.9×10^4
Coefficient of restitution, e	0.42	Contact damping coefficient, ζ	0.27
		Sliding friction, μ_s	0.5
		Rolling friction, μ_r	0.1
Stainless Steel (Impeller):			
Shear modulus, E (GPa)	200	Normal stiffness (N/m)	8.5×10^5
Poisson's ratio, v	0.3	Shear stiffness (N/m)	7.0×10^5
Glass (Vessel):			
Shear modulus, E (GPa)	70	Normal stiffness (N/m)	4.5×10^5
Poisson's ratio, v	0.3	Shear stiffness (N/m)	3.7×10^5
Global Properties:			
		Time step (s)	$7 – 8 \times 10^{-7}$

Table 2. Simulation condition sets used

Parameter	Values used
θ_{sec} (^{o})	10, 25, 40
n_d	2, 3, 4
d_{med} (mm)	2, 3, 4

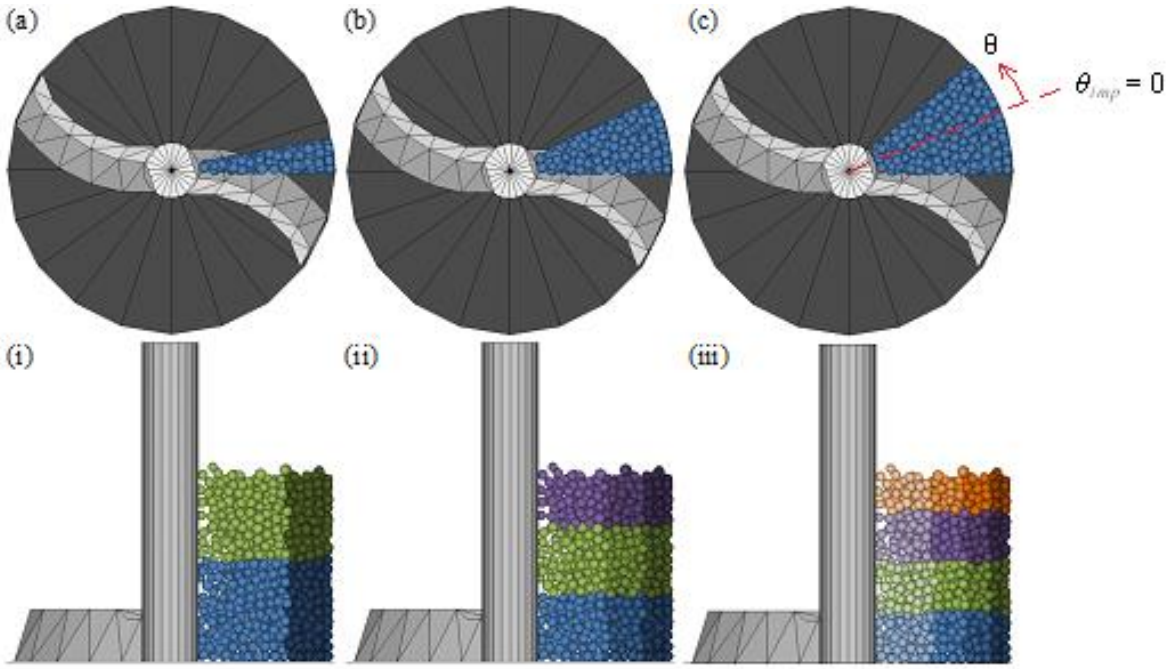

Figure 1. Measurement sectors and cells (a) θ_{sec} = 10^o (b) θ_{sec} = 25^o (c) θ_{sec} = 40^o (i) n_d = 2 (ii) n_d = 3 (iii) n_d = 4

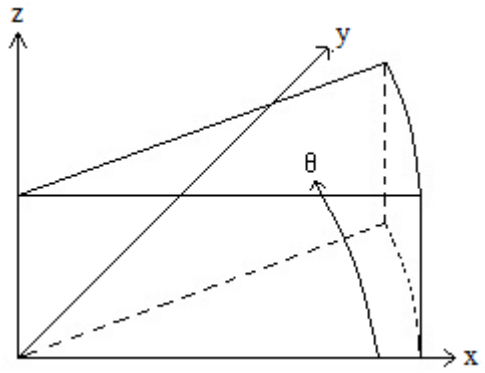

Figure 2. Axis direction definitions

3. Results and Discussion

In the simulated particle bed, the onset of agitation leads to a sudden increase in the deviatoric stress within the bed and the torque acting on the impeller. After two complete rotations the impeller torque reaches a cyclic steady-state condition [13]. The impeller is rotated in an anti-clockwise direction at a fixed impeller speed of 78 rpm. For the simulation conditions of d_{med} = 3 mm, $\theta_{sec} = 25^o$ and n_d = 3 (Figure 1b,ii), the variation of deviatoric stress with impeller position, θ_{imp}, in cell 3 is shown in Figure 3. When the tip of the first impeller blade is in the angular central line of the measurement sector, then $\theta_{imp} = 0^o$ (as shown in Figure 1). θ_{imp} increases as the impeller is rotated; the second blade reaches the angular centre of the measurement sector at $\theta_{imp} = 180^o$. As an impeller blade exits the measurement sector the deviatoric stress reduces to a negligible value, but it starts to rise again as the other impeller blade approaches the cell. The rise begins when the impeller blade is approximately 90^o from the angular centre of the measurement sector ($\theta_{imp} = 90^o$). The stress peaks slightly before the impeller blade reaches the angular centre of the measurement sector, and then decreases again as the blade passes through the measurement sector.

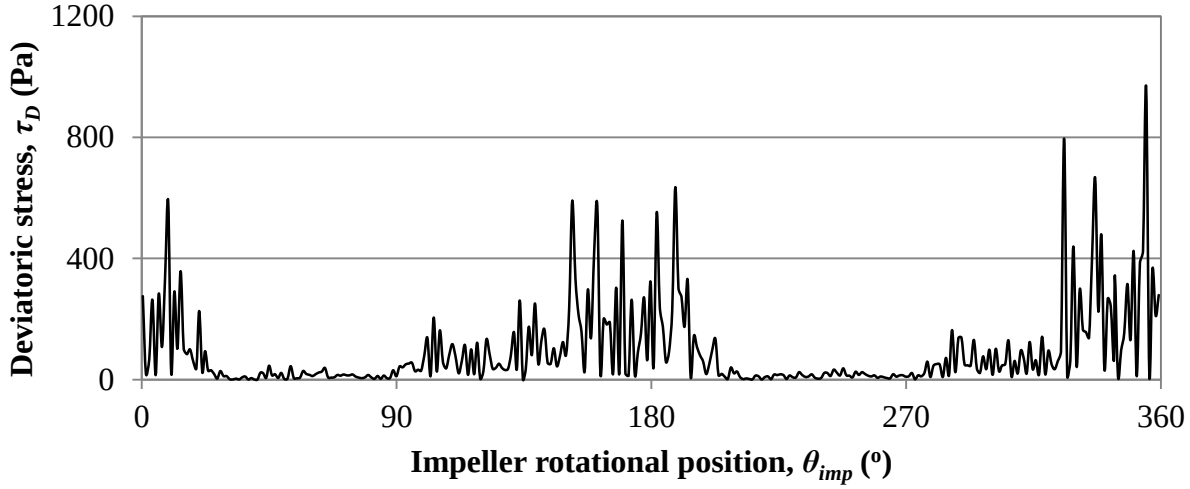

Figure 3. Deviatoric stress in cell 3 for $\theta_{sec} = 25^o$ and n_d = 3

The variation of deviatoric stress with impeller rotation is similar in all cells, though the magnitude of deviatoric stress varies. Figure 4 shows the arithmetic mean of the deviatoric stress calculated at a number of measurement intervals throughout one impeller rotation in each of the nine cells. The stresses increase with radial position throughout the bed and decrease with vertical position. It should be noted that the impeller height is approximately equal to the upper boundary of cells 1, 2 and 3. This explains the dramatic decrease in deviatoric stress above this boundary – from cells 1 – 3, to cells 4 - 9.

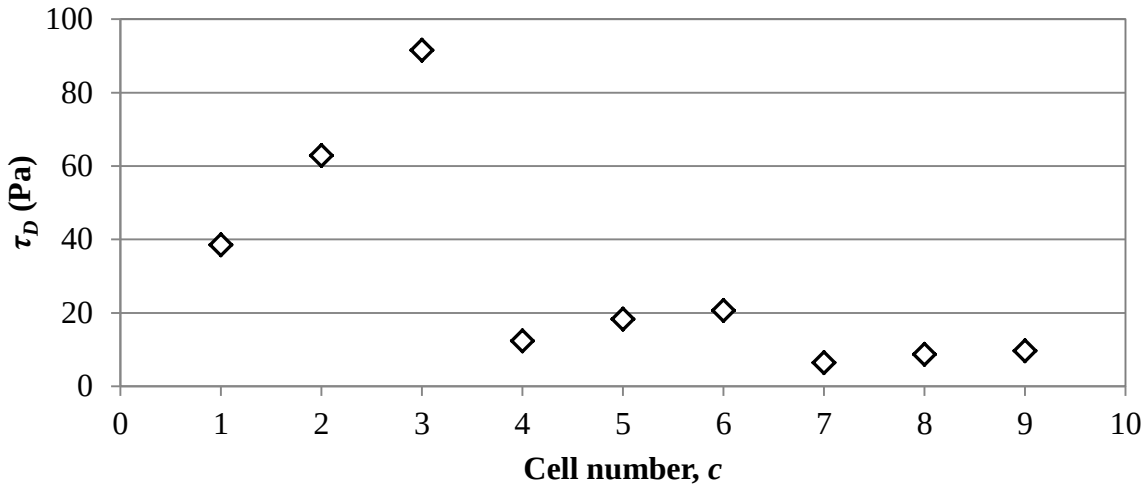

Figure 4. Average deviatoric stresses throughout one rotation for θ_{sec} = 25° and n_d = 3

The variation of strain rate in cell 3 with impeller position, using the same measurement system, is shown in Figure 5. The strain rate does not display such a significant variation with impeller position as does the deviatoric stress. The strain rate increases as the impeller approaches the measurement sector, and peaks slightly after the impeller reaches the angular centre of the measurement sector. This corresponds to the increased particle velocity in the immediate wake of the impeller blade. Following this peak, the strain rate decreases and remains relatively unchanged until the other impeller blade approaches.

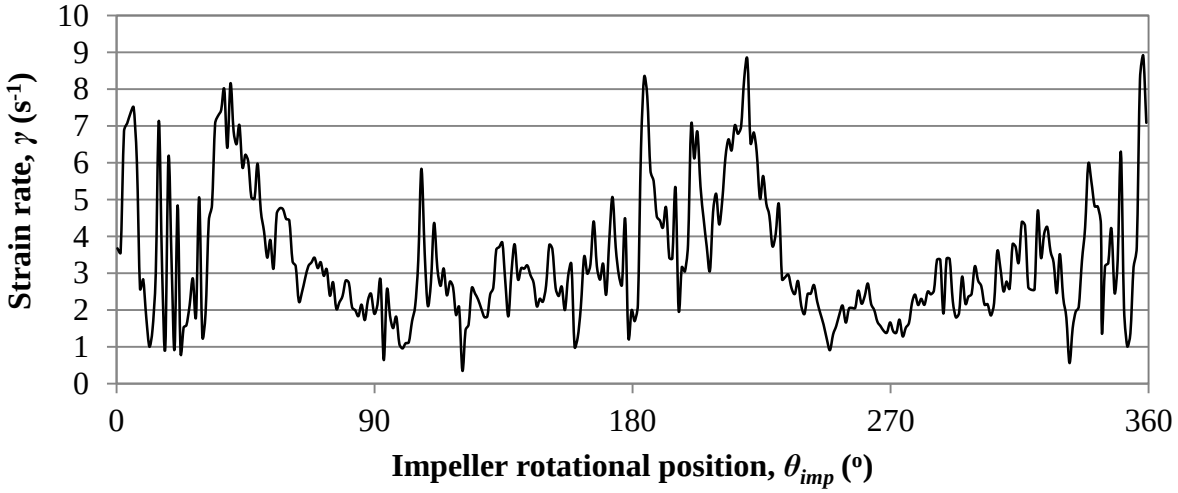

Figure 5. Strain rate in cell 3 for θ_{sec} = 25° and n_d = 3

The total strain in each cell after one impeller rotation is shown in Figure 6. The strain increases with radial position in a similar manner to the deviatoric stress. The strain decreases slightly with vertical position, though this decrease is significantly less pronounced than the decrease in deviatoric stress with vertical position.

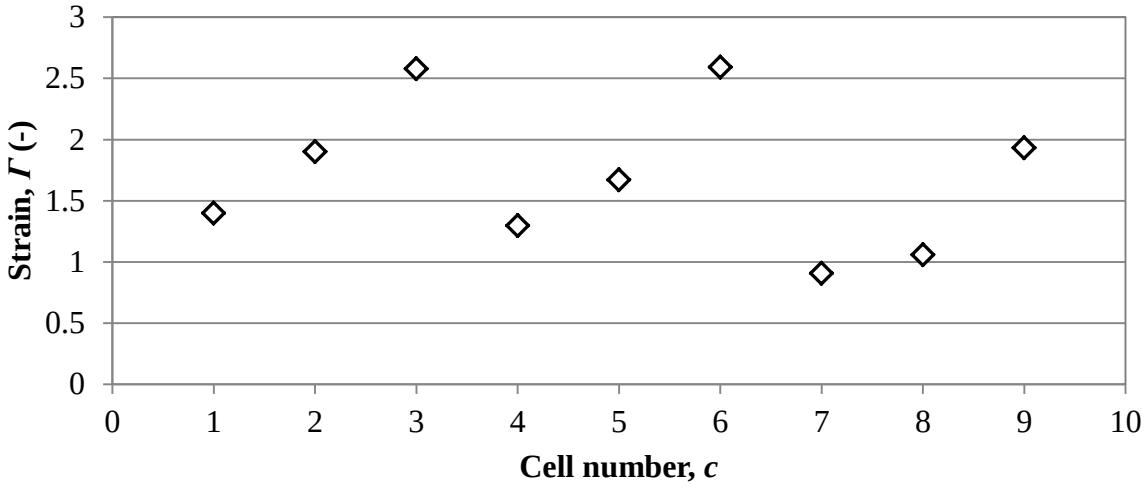

Figure 6. Total strain throughout one rotation for θ_{sec} = 25^o and n_d = 3

Throughout the course of the simulations with a median particle size of 3 mm, discussed above, the stresses and strain rates were measured for all combinations of θ_{sec} and n_d shown in Figure 1. The bed exhibits limited variation in packing fraction. Since the cells are of equal volume, the number of particles in each cell is approximately the same.

The influence of θ_{sec} on the average deviatoric stress in each cell was analysed for the case of n_d = 3. A decrease in the measurement sector size results in a slightly increased average deviatoric stress in the outer radial positions (cells 3, 6 and 9). This increase is most likely attributed to the reduction in the number of particles in a cell, which causes the stresses to be averaged by a smaller number of particles. Therefore the measured peak stresses are greater. However, this increase in stress is not noticeable in the majority of the bed.

The variation of total strain through one rotation with measurement sector size was analysed. As with the average deviatoric stress, the total strain increases when the measurement sector size is reduced. The total strain is slightly greater for θ_{sec} = 10^o as compared to 40^o in most of the measurement cells.

The average deviatoric stress obtained for each cell for n_d = 2 and 4 are shown in Figures 7 and 8, respectively. The stresses increase with radial position and decrease with vertical position in both cases, as in the case where n_d = 3. For the case of θ_{sec} = 25^o for n_d = 2, 3 and 4, the greatest average deviatoric stress in any cell is 56 Pa (Figure 7), 92 Pa (Figure 4) and 108 Pa (Figure 8), respectively. By comparing Figures 3, 7 and 8, it can be seen that as n_d is increased the greatest average deviatoric stress calculated in any of the cells increases.

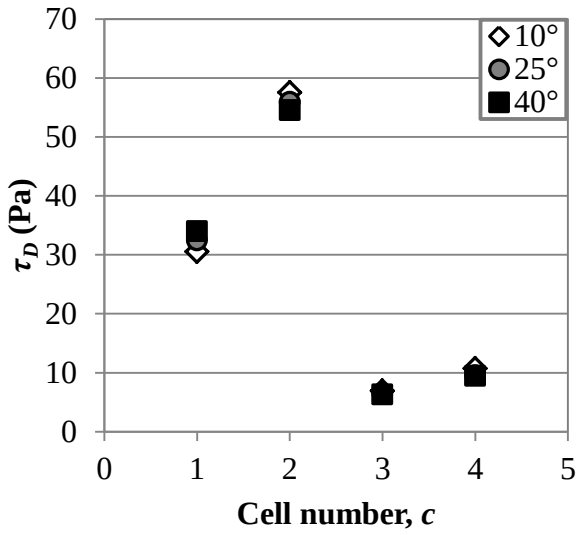

Figure 7. Average deviatoric stresses throughout one rotation for n_d = 2

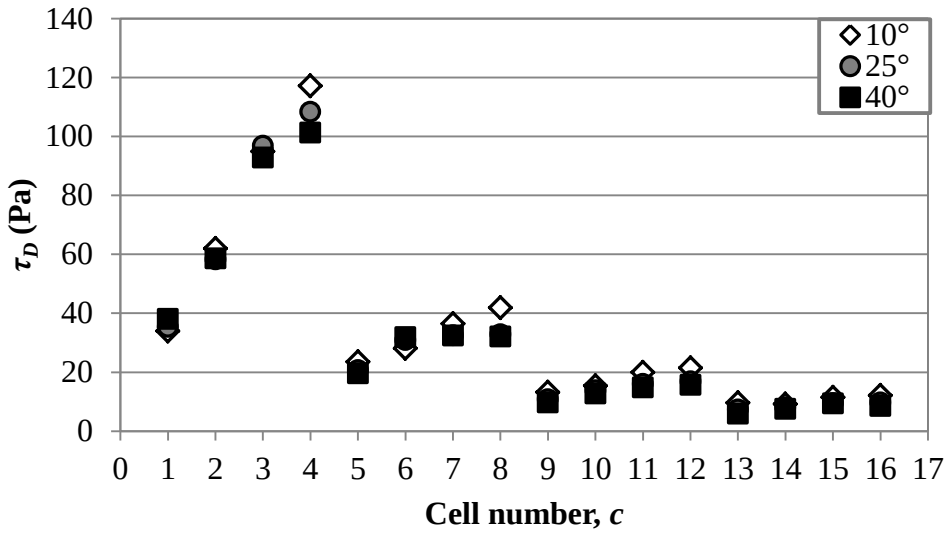

Figure 8. Average deviatoric stresses throughout one rotation for n_d = 4

Direct comparison of the deviatoric stresses between the different cases of n_d is difficult since the cell boundaries do not overlap in all cases. However, the cell boundaries of n_d = 2 do overlap with those of n_d = 4. As an example, cell 1 where n_d = 2 corresponds to the identical space as cells 1, 2, 5 and 6 where n_d = 4 (see Figure 1). By averaging the deviatoric stresses shown in Figure 8 so that they correspond to the identical measurement cells of n_d = 2, the influence of n_d on the deviatoric stresses can be ascertained. This comparison is shown in Figure 9. The average deviatoric stresses obtained when n_d = 4 are greater than those obtained when n_d = 2 throughout the entirety of the agitated bed.

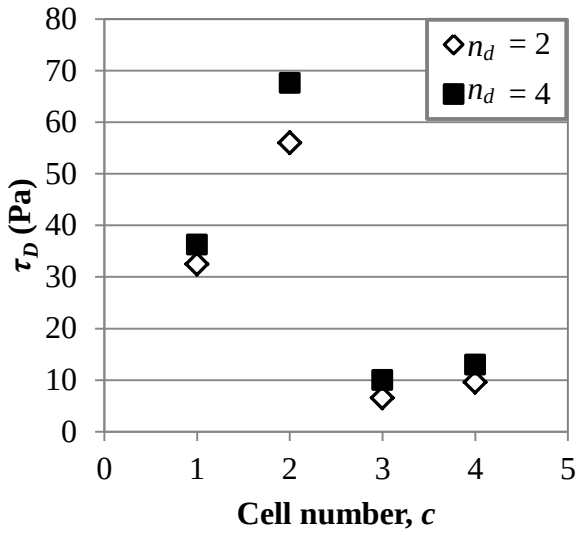

Figure 9. Average deviatoric stresses throughout one rotation for n_d = 2 compared to the average of corresponding cells where n_d = 4

The total strains in each cell after one impeller rotation have also been calculated. When n_d = 2 the total strain increases with radial position and decreases slightly with vertical position, in a similar manner to when n_d = 3. Though direct comparison between these two cases is difficult, the strain does appear to be generally increased when n_d is increased. For the cases of n_d = 2, 3 and 4 the overall trends of total strain are similar.

The influence of simulation particle size on the estimated stresses and strains is considered next. The median particle diameter, d_{med}, is varied between 2, 3 and 4 mm in separate simulations. In all cases the span of the distribution is fixed at 0.18, corresponding to that of the experimental Paracetamol. For comparison of simulation particle size, the measurement system of $\theta_{sec} = 25^o$ and n_d = 3 is considered. The variation in the average deviatoric stress in each measurement cell with particle size is shown in Figure 10. An increase in particle size causes an increase in the deviatoric stress for all cells. The average number of particles per cell is very similar in the two cases of (d_{med} = 3 mm; n_d = 2), and (d_{med} = 2 mm; n_d = 4). Since the boundaries of the cells where n_d = 2 overlap with boundaries for n_d = 4, the average stresses in the corresponding cells can be compared, using the same approach of that for Figure 9. The average deviatoric stresses are found to be strikingly similar in every measurement cell for these two cases, as they have a similar number of particles. This suggests that the increase in calculated stress with an increase in particle size is due to the reduction in the average number of particles in each cell. Therefore the deviatoric stress is determined by the size of the cell dimensions relative to the particle size.

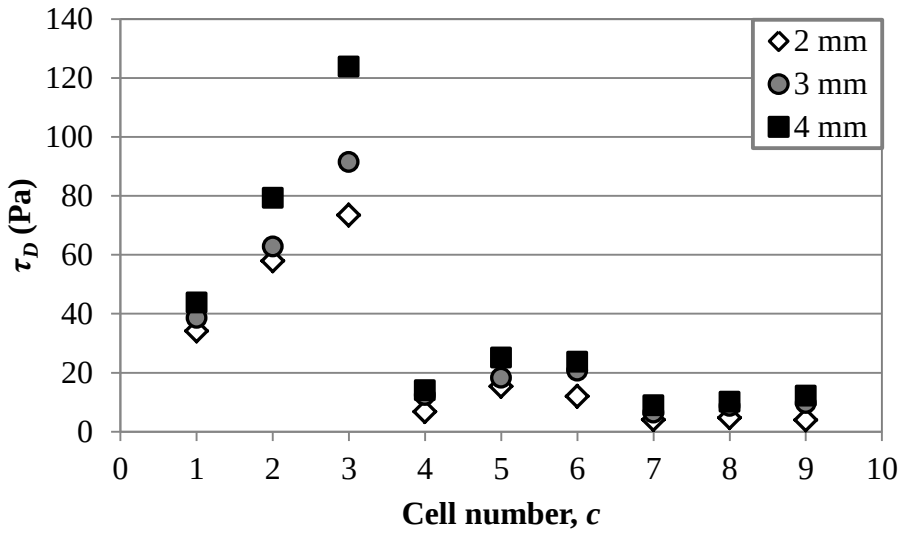

Figure 10. Average deviatoric stresses throughout one rotation for θ_{sec} = 25° and n_d = 3

The total strain in each cell after one impeller rotation is shown in Figure 11 for median particle sizes of 2, 3 and 4 mm. As with the average deviatoric stress, the total strain increases with particle size throughout the majority of the bed.

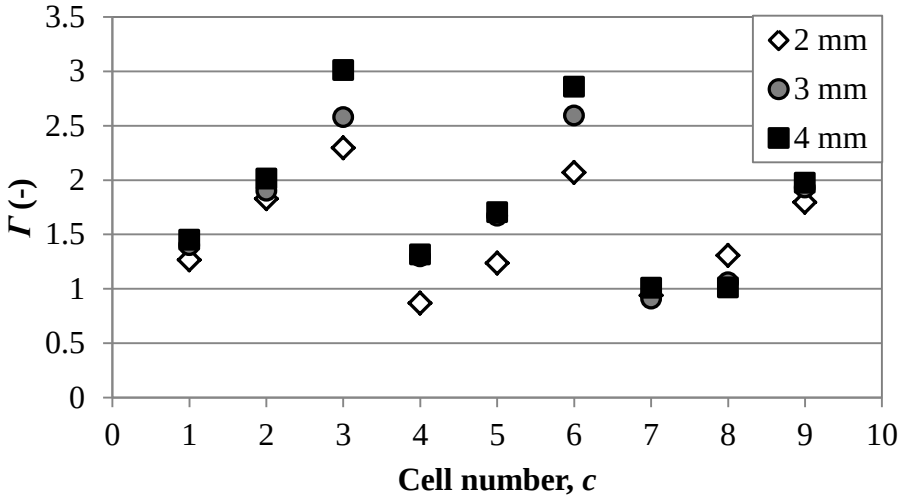

Figure 11. Total strain throughout one rotation for θ_{sec} = 25° and n_d = 3

The calculated values of deviatoric stress and strain rate in each cell, at each interval, are utilised in Eq. 6 to predict the attrition occurring due to one impeller rotation. The values of τ_{ref}, K_N, φ and β have been experimentally determined by Eq. 5 from measurements of Paracetamol attrition at a range of shear stresses and strains, and are equal to 0.183 MPa, 0.71, 1.28 and 0.49, respectively [13]. From the prediction of the attrition occurring due to one impeller rotation (Eq. 6), the attrition occurring after I rotations is given by Eq. 8. An increase in deviatoric stress or strain rate will result in an increase in $W_{I=1}$, as shown by Eqs. 6 and 7 and therefore an increase in W_I (Eq. 8). Table 3 shows the variation in predicted attrition after one impeller rotation, $W_{I=1,}$ for d_{med} = 3mm as a result of varying the

measurement sector size and the number of divisions within. An increase in sector size causes a slight decrease in predicted attrition, as a result of the reduction in total strain and a slight reduction in deviatoric stress. However, the variation in predicted attrition with sector size is not substantial; an increase in sector size from 10^o to 25^o causes the predicted attrition to decrease by 2-6 %. As n_d is increased the predicted attrition increases significantly. An increase in n_d from 2 to 3 results in a 15-23 % increase in the predicted attrition. This is a more substantial effect than a 15^o change in the measurement sector size. Direct comparison of the stresses and strains calculated with different values of n_d is difficult. However the stresses and strains do generally increase as n_d is increased. This increase appears to be due to the reduction in the number of particles in each cell, which makes the calculation more dependent on each individual particle. Therefore, if a localised high stress region falls within a cell the average stress is greater when the cell size approximates the size of this high stress region. As the cell size is increased to include more particles experiencing a lower stress, the average stress calculated for this cell decreases.

Table 3. Predicted attrition after one impeller rotation, $W_{I=1}$ ($\times 10^{-2}$), for d_{med} = 3 mm

θ_{sec} (^{o})	n_d		
	2	3	4
10	0.99	1.21	1.28
25	0.97	1.14	1.24
40	0.96	1.11	1.13

Another factor affecting the number of particles in each measurement cell is the median particle size. Table 4 shows the variation in predicted attrition after one impeller rotation, $W_{I=1,}$ for $\theta_{sec} = 25^o$ as a result of varying the median particle size and the number of divisions within the measurement sector. When the median particle size is increased the predicted attrition increases. In such a case the average number of particles per measurement cell is reduced, and hence the calculated stresses are increased. Varying the median particle size from 3 mm to 2 or 4 mm leads to a change in the predicted attrition of up to 20 %.

Table 4. Predicted attrition after one impeller rotation, $W_{I=1}$ ($\times 10^{-2}$), for θ_{sec} = 25 ^{o}

d_{med} (mm)	n_d		
	2	3	4
2	0.80	0.95	0.97
3	0.97	1.14	1.24
4	1.08	1.35	1.43

It is apparent that the average number of particles per measurement cell has a substantial effect on the predicted attrition. Figure 12 shows the predicted attrition after one impeller rotation for all cases of d_{med}, θ_{sec} and n_d. The average number of particles per cell, $N_{p,ave}$, varies between these different measurement systems. It is clear that an increase in the number of particles per cell generally causes a reduction in the predicted attrition. However, the predicted attrition is slightly less for the 10^o sector size for a given number of $N_{p,ave}$. The initial case of d_{med} = 3 mm, $\theta_{sec} = 25^o$ and n_d = 3, utilised by Hare *et al.* [13], provides a very good agreement with the experimental data. In this case the cell dimensions are in the range

of 4 – 8 particle diameters, which are comparable to the width of a naturally occurring shear band. It therefore seems logical that when applying cells with prescribed volumes to DEM, the cell dimensions should be relevant to the phenomena of interest. If the system experiences shear deformation, the measurement cell dimensions should be comparable to the dimensions of a naturally occurring shear band. This has far reaching implications for the assessment of internal stresses in a particle bed, as the length-scale of the averaging procedure should be carefully considered.

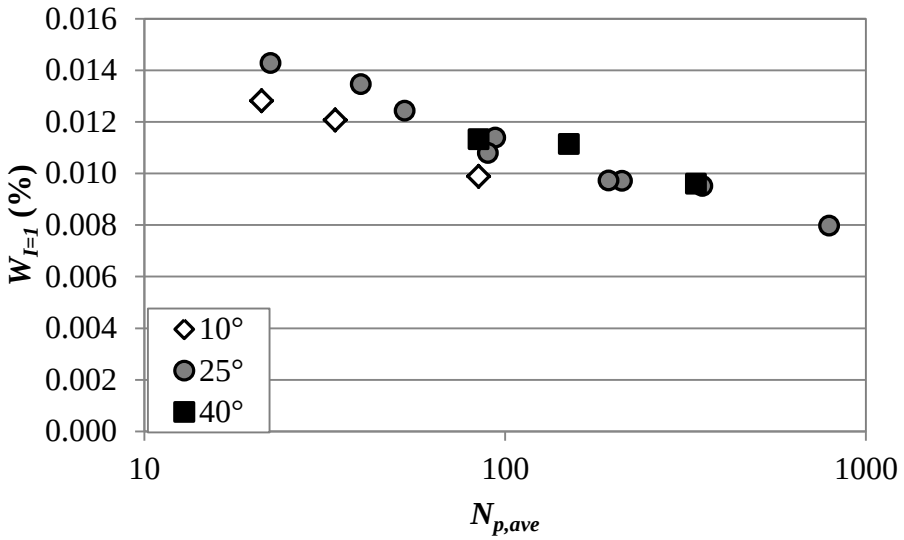

Figure 12. Influence of the average number of particles per cell on the predicted attrition after one impeller rotation

4. Conclusions

Particle breakage in agitated vessels occurs due to the shear stresses and strains caused by the impeller motion. A method to predict the extent of breakage by analysing the stress and strain rate distributions in a DEM simulation of the bed has been introduced. The stresses and strain rates are estimated within a sector of the bed throughout one impeller rotation. This sector is divided radially and vertically into a number of cells. The dimensions of the cells have been shown to be influential in estimating the magnitude of stresses and strain rates within. An increase in the number of radial and vertical divisions, or the median particle size, results in an increase in the predicted attrition. In all these cases the average number of particles in each cell is reduced, therefore calculation of stress is more dependent on individual particles. This means that in the high stress regions of the bed the cells no longer include particles that experience a low stress. Consequently the calculated stresses and extent of attrition prediction increase.

The predicted attrition was compared to the experimentally determined breakage in the agitated vessel [13]. The prediction was most accurate when the dimensions of the measurement cells were comparable with the width of a naturally occurring shear band. Since the breakage is caused by shear deformation, the stresses and strain rates over these

length scales determine the extent of breakage. A wider implication is that when taking average values within measurement cells, the dimensions of these cells should be representative of the phenomena occurring in the system.

Acknowledgements

This work was funded by an Industrial Case Award funded by the EPSRC and GlaxoSmithKline. This funding is gratefully acknowledged. The project was co-ordinated by Dr Robert Dennehy. The authors are thankful for his support.

Nomenclature

c	measurement volume number
d_{med}	median particle diameter
d_s	particle sieve size
e	coefficient of restitution
E	shear modulus
F	force
I	impeller rotations
k_N	empirical constant in Neil and Bridgwater relation
K	stiffness
n	interval
n_d	number of radial and vertical divisions
$N_{p,ave}$	number of particles in a measurement volume
r	radial position
r_p	particle radius
t	time
v	velocity
V	volume
W	Extent of attrition
z	vertical position
β	rate of material degradation in Neil and Bridgwater relation
γ	strain rate
Γ	strain
ζ	contact damping coefficient
θ_{imp}	angular rotation of the impeller
θ_{sec}	measurement sector angle
ν	Poisson's ratio
ρ	density
σ	stress
τ	shear stress
τ_D	deviatoric stress
φ	relative influence of strain and stress in Neil and Bridgwater relation
χ	mass fraction

subscripts

ii	in the *i* direction on the *i* face
I=1	after one impeller rotation
n	normal
ref	reference
s	shear
SCS	side-crushing
xx	in the *x* direction on the *x* face
yy	in the *y* direction on the *y* face
zz	in the *z* direction on the *z* face
θ	in the θ direction

References

[1] D.J. Stephens, J. Bridgwater, 1978, The mixing and segregation of cohesionless particulate materials Part I. Failure Zone Formation, Powder Technology, 21, 17-28.

[2] S.J. Antony, M.R. Kuhn, 2004, Influence of particle shape on granular contact signatures and shear strength: new insights from simulations, International Journal of Solids and Structures, 41, 5863-5870.

[3] F. Radjai, D.E. Wolf, M. Jean, J.J. Moreau, 1998, Bimodal character of stress transitions in granular packings, Physical Review Letters, 80(1), 61-64.

[4] A. Hassanpour, Y. Ding, M. Ghadiri, 2004, Shear deformation of binary mixtures of dry particulate solids, Advanced Powder Technology, 15(6), 687-697.

[5] N.P. Kruyt, S.J. Antony, 2007, Force, relative displacement, and work networks in granular materials subjected to quasistatic deformation, Physical Review E, 75(5) 051308.

[6] Z. Ning, M. Ghadiri, 2006, Distinct element analysis of attrition of granular solids under shear deformation, Chemical Engineering Science, 61, 5991-6001.

[7] J.E. Gwyn, 1969, On the particle size distribution function and the attrition of cracking catalysts, American Institute of Chemical Engineers, 15, 35-39.

[8] B.K. Paramanathan, J. Bridgwater, 1983, Attrition of solids-I cell development, Chemical Engineering Science, 38 (2), 197-206.

[9] C.E. Ouwerkerk, 1991, A micro-mechanical connection between single-particle strength and the bulk strength of random packings of spherical particles, Powder Technology, 65, 125-138.

[10] M. Ghadiri, Z. Ning, S.J. Kenter, E. Puik, 2000, Attrition of granular solids in a shear cell, Chemical Engineering Science, 55, 5445-5456.

[11] A.U. Neil, J. Bridgwater, 1994, Attrition of particulate solids under shear, Powder Technology, 65, 125-138.

[12] J. Bridgwater, R. Utsumi, Z. Zhang, T. Tuladhar, 2003, Particle attrition due to shearing-the effects of stress, strain and particle shape, Chemical Engineering Science, 58 (20), 4649-4665.

[13] C. Hare, M. Ghadiri, R. Dennehy, 2011, Prediction of attrition in agitated particle beds, Chemical Engineering Science, 66, 4757-4770.
[14] K. Bagi, 1996, Stress and strain in granular assemblies, Mechanics of Materials, 22, 165-177.
[15] S. Luding, 2008, Constitutive relations for the shear band evolution in granular matter under large strain, Particuology, 6, 501-505.
[16] M. Depken, W. van Saarloos, M. van Hecke, 2006, Continuum approach to wide shear zones in quasistatic granular matter, Physical Review E, 73, 031302.
[17] A. Hassanpour, C.C. Kwan, B.H. Ng, N. Rahmanian, Y. Ding, S.J. Antony, X.D. Jia, M. Ghadiri, 2009, Effect of granulation scale-up on the strength of granules, Powder Technology, 189, 304-312.
[18] A. Hassanpour, H.S. Tan, A. Bayly, P. Gopalkrishnan, B.H. Ng, M. Ghadiri, 2011, Analysis of particle motion in a paddle mixer using Discrete Element Method (DEM), Powder Technology, 206, 189-194.